NASA/TM—2005-213602

Quadrant CFD Analysis of a Mixer-Ejector Nozzle for HSCT Applications

Dennis A. Yoder, Nicholas J. Georgiadis, and John D. Wolter
Glenn Research Center, Cleveland, Ohio

April 2005

The NASA STI Program Office . . . in Profile

Since its founding, NASA has been dedicated to the advancement of aeronautics and space science. The NASA Scientific and Technical Information (STI) Program Office plays a key part in helping NASA maintain this important role.

The NASA STI Program Office is operated by Langley Research Center, the Lead Center for NASA's scientific and technical information. The NASA STI Program Office provides access to the NASA STI Database, the largest collection of aeronautical and space science STI in the world. The Program Office is also NASA's institutional mechanism for disseminating the results of its research and development activities. These results are published by NASA in the NASA STI Report Series, which includes the following report types:

- TECHNICAL PUBLICATION. Reports of completed research or a major significant phase of research that present the results of NASA programs and include extensive data or theoretical analysis. Includes compilations of significant scientific and technical data and information deemed to be of continuing reference value. NASA's counterpart of peer-reviewed formal professional papers but has less stringent limitations on manuscript length and extent of graphic presentations.

- TECHNICAL MEMORANDUM. Scientific and technical findings that are preliminary or of specialized interest, e.g., quick release reports, working papers, and bibliographies that contain minimal annotation. Does not contain extensive analysis.

- CONTRACTOR REPORT. Scientific and technical findings by NASA-sponsored contractors and grantees.

- CONFERENCE PUBLICATION. Collected papers from scientific and technical conferences, symposia, seminars, or other meetings sponsored or cosponsored by NASA.

- SPECIAL PUBLICATION. Scientific, technical, or historical information from NASA programs, projects, and missions, often concerned with subjects having substantial public interest.

- TECHNICAL TRANSLATION. English-language translations of foreign scientific and technical material pertinent to NASA's mission.

Specialized services that complement the STI Program Office's diverse offerings include creating custom thesauri, building customized databases, organizing and publishing research results . . . even providing videos.

For more information about the NASA STI Program Office, see the following:

- Access the NASA STI Program Home Page at ***http://www.sti.nasa.gov***

- E-mail your question via the Internet to help@sti.nasa.gov

- Fax your question to the NASA Access Help Desk at 301–621–0134

- Telephone the NASA Access Help Desk at 301–621–0390

- Write to:
  NASA Access Help Desk
  NASA Center for AeroSpace Information
  7121 Standard Drive
  Hanover, MD 21076

NASA/TM—2005-213602

Quadrant CFD Analysis of a Mixer-Ejector Nozzle for HSCT Applications

Dennis A. Yoder, Nickolas J. Georgiadis, and John D. Wolter
Glenn Research Center, Cleveland, Ohio

National Aeronautics and
Space Administration

Glenn Research Center

April 2005

Document History

This research was originally published internally as HSR071 in September 1999.

Trade names or manufacturers' names are used in this report for identification only. This usage does not constitute an official endorsement, either expressed or implied, by the National Aeronautics and Space Administration.

Available from

NASA Center for Aerospace Information
7121 Standard Drive
Hanover, MD 21076

National Technical Information Service
5285 Port Royal Road
Springfield, VA 22100

Available electronically at http://gltrs.grc.nasa.gov

Quadrant CFD Analyses of a Mixer-Ejector Nozzle for HSCT Applications

Dennis A. Yoder, Nicholas J. Georgiadis, and John D. Wolter
National Aeronautics and Space Administration
Glenn Research Center
Cleveland, Ohio 44135

Abstract

This study investigates the sidewall effect on flow within the mixing duct downstream of a lobed mixer-ejector nozzle. Simulations which model only one half-chute width of the ejector array are compared with those which model one complete quadrant of the nozzle geometry and with available experimental data. These solutions demonstrate the applicability of the half-chute technique to model the flowfield far away from the sidewall and the necessity of a full-quadrant simulation to predict the formation of a low-energy flow region near the sidewall. The quadrant solutions are further examined to determine the cause of this low-energy region, which reduces the amount of mixing and lowers the thrust of the nozzle. Grid resolution and different grid topologies are also examined. Finally, an assessment of the half-chute and quadrant approaches is made to determine the ability of these simulations to provide qualitative and/or quantitative predictions for this type of complex flowfield.

Nomenclature

C_{fg}	Gross Thrust Coefficient, $F_g/\dot{m}_p V_{p_{ideal}}$
CER	Chute Area Expansion Ratio
F_g	Gross Thrust
H	Mixing Duct Height
L	Mixing Duct Length (Mixer Exit Plane to Duct Exit Plane)
$\dot{m}_p$	Primary Mass Flow Rate
$\dot{m}_s$	Secondary Mass Flow Rate
MAR	Mixer Area Ratio
NPR	Nozzle Pressure Ratio
PEN	Mixer Penetration
SAR	Suppressor Area Ratio
$V_{p_{ideal}}$	Ideal Unsuppressed Primary Jet Velocity
W	Mixing Duct Width
x	Axial Distance from Mixer Exit Plane
y	Span-wise Distance from Center of Mixing Duct
z	Vertical Distance from Center of Mixing Duct
γ	Ratio of Specific Heats
Ω	Axial Vorticity
ω	Pumping Ratio, $\dot{m}_s/\dot{m}_p$

Introduction

For several years, NASA's High-Speed Research (HSR) program investigated methods for jet engine noise suppression. All future High Speed Civil Transport (HSCT) aircraft will be required to meet stringent community noise regulations, particularly at the takeoff condition where maximum engine thrust is necessary.

One concept for reducing jet exhaust noise that has received significant attention is the lobed mixer-ejector nozzle, such as that shown in figure 1. Hot primary flow from the engine is combined with lower energy freestream air entrained through the secondary flow chutes. After passing through a mixing section, the combined flow has a lower nozzle exit velocity and consequently produces lower noise levels. However, the ejector process enhances the mass flow rate such that the resultant thrust remains acceptably high. At cruise conditions, the secondary inlet is closed to allow optimum performance of the nozzle over a large portion of the flight envelope.

Evaluation and testing of these mixer-ejector nozzle concepts is both difficult and expensive. Since both performance and acoustic data are needed to evaluate these nozzles, they must be tested in an acoustic facility that has a quality thrust balance.

In addition, these configurations involve a complex series of mixer chutes that are difficult and costly to fabricate. Stereo lithography has been used successfully to reduce these fabrication costs, but models made with this material can not withstand the high temperatures of the primary flow from the engine. This limits its usefulness to cold-flow performance (i.e., non-acoustic) testing.

Computational fluid dynamics (CFD) can be used to perform preliminary analyses to identify the relative performance of different nozzle concepts. This information can be used to downselect concepts for testing in one of the experimental facilities. In particular, CFD can be used to perform chute-shaping studies and evaluate the effect of lobe count.

However, CFD has not been fully validated for complex mixer-ejector nozzles. Because of the large number of grid points needed to accurately resolve a complete quadrant of the nozzle and the complexity of the grid generation task, most preliminary analyses are performed using a region which only extends across one half-chute width in the span-wise direction. This half-chute approach, in which the computational domain extends from the peak of the primary flow chute to the trough of the nearest secondary flow chute, assumes symmetry in the span-wise direction. As a result, any effect on the flow due to the presence of the sidewall is absent.

Experimental measurements[1] of the mixer-ejector configuration shown schematically in figure 1 indicate the presence of a low energy region which forms along the sidewall near the xy-symmetry plane. This region of low energy flow is undesirable, because it results in lower thrust and higher noise levels than would a flow that is more fully mixed.

In this study, CFD will be used to investigate the effect of the sidewall on the flow within the mixing duct and attempt to explain the formation of this low energy region. Solutions from half-chute and full-quadrant simulations of the nozzle will be compared to ascertain the validity of the symmetry assumption away from the sidewall and the loss in accuracy of not including these sidewall effects. In addition, the issues of grid resolution, grid topology, and the ability of CFD to make qualitative and/or quantitative predictions for these complex flowfields will be addressed.

Geometry and Flow Conditions

The mixer-ejector nozzle being modeled is the Down Stream Mixer (DSM) with mixer number 9 which was tested experimentally at the Boeing Low Speed Aeroacoustic Facility (LSAF).[1] As shown in figure 1, both the top and bottom mixer-chute arrays contain 9 primary and 10 secondary chutes across the width of the nozzle. Near the sidewalls, the secondary chute contains an extra region that extends roughly one half-chute width in the span-wise direction. This type of chute design, referred to as a full-cold chute along the sidewall, was designed to entrain additional secondary mass flow and reduce thermal stress on the sidewalls. For this particular configuration, the primary chute also extends to the sidewall. This nozzle is further characterized as having a mixer area ratio (MAR) of 0.90, a suppressor area ratio (SAR) of 2.9, an area Chute Expansion Ratio (CER) of 1.06, and a penetration (PEN) of 92.5%. Figure 2 illustrates how these parameters are defined. Only the untreated hardwall configuration (e.g., no acoustic liners) was modeled numerically. This corresponds to configuration 953.576 in the test matrix listed in reference 1.

The flow conditions simulated were as follows: the total temperature of the primary nozzle flow was set to 1551 degrees Rankine and the nozzle was operated at a primary nozzle pressure ratio (NPR) of 3.43. The freestream temperature and pressure were set to 14.83 psi and 518.69 degrees Rankine. While the experimental data were obtained statically, the CFD analysis was performed at a freestream Mach number of 0.07 to enhance the stability and convergence rate of the code. This resulted in only a 0.3 percent increase in freestream total pressure.

Experimental data are available for the pumping ratio and thrust. Surveys of the axial velocity and total temperature were also measured at the duct exit plane using a 5 hole probe. These surveys were only taken in one of the quadrants of the duct. Within this quadrant, the survey mesh contained eight points in the y-direction and seven points in the z-direction. For the results presented here, this data has been reflected to the other quadrants to provide contours over the entire duct exit area.

Computational Domain

Figure 3 is a sketch denoting the computational domain over which these calculations were performed. The inflow boundary for the primary nozzle was placed slighty upstream of the ejector array and uniform values for total temperature and pressure were specified at the engine interface. Freestream conditions were specified for flow external to the nozzle, which created a pressure gradient in the secondary inlet and allowed for the entrainment of

air into the mixing duct. The outflow boundary was placed several duct heights downstream of the duct exit plane.

For the quadrant simulations, the internal sidewall along the primary and secondary flow passages and the mixing duct was modeled as well as the freestream flow over the external shroud surface and flap. These surfaces were treated as adiabatic viscous walls.

For the half-chute calculations, the computational domain consisted of the half-chute region nearest the xz-symmetry plane (y=0). As illustrated in figure 4, this region extends from the peak of the center primary chute to the trough of the closest secondary chute. An additional symmetry condition was imposed along the xz-plane that runs through the trough of the secondary chute. None of the other chutes, the internal sidewall, or the external shroud surface were modeled. Freestream flow through the secondary inlet and over the external flap surface was included in these calculations.

In the results to be presented, the half-chute solutions were reflected and copied several times in the y-direction so that a more direct comparison with the quadrant solutions could be made. Contours at the duct exit plane are presented over the entire width and height of the mixing duct. These were generated by further reflecting the solutions to fill the other quadrants of the duct.

Computational Algorithm

Calculations were performed using the NPARC finite difference code,[2] which solves the conservation law form of the Reynolds-averaged Navier-Stokes equations. Steady state solutions were obtained with an approximate factorization algorithm and second order accurate central differencing in the spatial direction. Artificial dissipation was used to keep the algorithm stable. The two-equation Chien[3] k-ϵ turbulence model was used, but no corrections for compressibility or vortex stretching were included for these calculations. The flow was assumed to behave as a perfect gas with γ=1.4.

Convergence criteria for these cases included monitoring of the L2 residual as well as integral flow quantities such as mass flow through the mixing duct, thrust coefficients, and pumping ratio. Solutions were deemed to reach steady-state once a three-order reduction in residual had been achieved, mass flow rate through the mixing duct was conserved within 0.5%, and the resultant values for the pumping and thrust appeared stable.

Initial Comparisons

Since the aim of the initial half-chute and quadrant calculations was to determine the ability of CFD to predict the formation of the low energy region near the sidewall, but not necessarily the finer details of the flowfield, these calculations were conducted on coarse grids. The half-chute grid contained 133,938 points, while the quadrant mesh contained roughly 1.3 million points. Packing of grid points to y^+ values of 1 near the viscous walls of the mixer lobes and secondary inlet was not strictly enforced. Table 1 presents a breakdown of how these grid points were distributed throughout each region of the mesh.

Figure 5 compares the axial velocity at the duct exit plane as predicted using the half-chute and quadrant approaches on these coarse meshes. The comparison is significant because the ability of the quadrant simulation to predict the formation of the velocity deficit regions along the sidewalls is demonstrated. However, the results also indicate a strong three-dimensional effect along the xz-symmetry plane which the half-chute approximation is unable to predict and which is not evident in the experimental data. Further examination of the coarse grid solutions indicated that this was due to deficiencies in the coarse grids used in these computations.

Grid Refinement Issues

Within the mixer, construction of the computational mesh was such that the mixer lobe was described by a single grid line in the span-wise direction, while the opposing grid line followed the xy-symmetry plane (z=0). This grid topology, which is shown schematically in figure 6(a) for a primary chute, contains a significant amount of grid skewness. Furthermore, the grid clustering needed to resolve the peak of the primary chute results in a large number of points away from the wall.

While the grid within the mixing duct was intentionally designed to be coarse, the poor grid resolution appears to cause a rapid decay of the high-energy flow from the central primary chute. For the half-chute calculation, this effect is not apparent, most likely due to the imposition of the symmetry boundary condition. For the quadrant solution, however, the three-dimensional effects are stronger. This, coupled with the coarse grid and the fact that points along the xz-symmetry plane are dominated by the symmetry condition, resulted in the velocity deficit region along the xz-symmetry

plane. Spacing of the grid points in the mixing duct near-wall regions was found to yield an average y^+ value of 5.

Grid difficulties were also identified with the two grid blocks that compose the plume region. The core of the jet was contained in a rectangular grid which had a cross-flow area roughly twice that of the duct exit. A coarser cylindrical grid wrapped around this core mesh and was used to model the freestream. One concern of this grid structure is that the interface between blocks may not lie far enough away from the shear layer, thereby influencing the decay of the jet.

Because of the shortcomings identified in the coarse meshes, the second set of calculations was done on a new set of grids rather than finer versions of the first grids. These grids were designed to correct the aforementioned problems as well as to provide better overall grid resolution. Table 1 compares the grid point distribution for each of the major flow regions with those used in the initial study. Resolution of the mixing duct was increased by more than a factor of five, while the total number of points was increased by a factor of three.

Within the primary and secondary mixer chutes, an entirely different grid topology was chosen in order to reduce the amount of grid skewness and to improve the near-wall resolution. This new grid structure, which is illustrated in figure 6(b) for a primary flow chute, divides each lobe into two parts - a base region and a chute region. While some points are clustered toward the block interface, the majority are located along the viscous surface of the lobe. In addition, the overall grid skewness has been significantly reduced. However, there is still a small region of localized grid skewness near the peak of the primary chute which is difficult to overcome.

The structure of the rectangular grid used within the mixing duct was not altered. However, the number of points was increased significantly in order to provide better resolution. In the (span-wise) y-direction, for example, the number of points was increased by roughly a factor of four to give 33 points across each half-chute width. The near-wall grid spacing was also enhanced slightly, resulting in an average y^+ of about 1.5. The maximum grid stretching ratio was approximately 1.3.

A single rectangular grid was used to model the entire plume region. This ensured that the block boundaries were far enough away from the jet to not influence the decay rate. Points were clustered in the y-direction near the sidewall trailing edge and in the z-direction near the flap trailing edge to resolve the jet shear layer.

Results

Figure 7 compares the axial velocity contours inside the mixing duct predicted using the coarse- and fine-mesh quadrant grids. This figure clearly shows that the high-energy flow from the center primary chute dissipates very quickly in the coarse-mesh solution, leaving a velocity deficit region along the xz-symmetry plane. It is also interesting to note that the coarse-mesh solution predicts that the high-energy flow from the primary chutes propagates toward the xy-symmetry plane, while the fine-mesh solution indicates that it actually moves away from that plane. This difference between solutions appears to be caused by differences in the prediction of the sidewall near-wall flow region. At the x/L=0.25 location, the fine-mesh solution reveals a larger velocity deficit region near the center of the sidewall, which causes the high-energy streaks from the primary stream to separate from the primary core-flow region near the xy-symmetry plane. These high-energy streaks then coalesce as they propagate downstream, while the core-flow appears to dissipate.

The axial velocity contours at the duct exit plane are compared with the experimental data in figure 8. The top half of this figure, which compares the coarse-mesh half-chute and quadrant solutions, are the same results presented in figure 5. While the coarse-mesh quadrant solution is able to predict the formation of velocity deficit regions along the sidewalls, it also indicates a strong three-dimensional effect along the xz-symmetry plane which the half-chute approximation is unable to predict and which is not evident in the experimental data.

The fine-mesh quadrant solution provides much better agreement with the experimental data than does the coarse-mesh solution. Also note that the size and shape of the low velocity region appears to be well predicted. Examination of the fine-mesh quadrant solution along the xz-symmetry plane indicates that it behaves very much like that of the fine-mesh half-chute solution. This indicates that three-dimensional effects near the y=0 symmetry plane are small.

Figure 9 compares the axial velocity profiles at the duct exit plane along the z=0 and y=0 symmetry cuts. It was previously noted that the coarse-grid solution predicted that the high-energy flow from the primary chutes propagated toward the xy-symmetry plane (z=0). This fact is evident in the profile plot, where the coarse-mesh velocity values along the z=0 cut are found to be much higher than the

experimental data. Furthermore, it was noted that the high-energy flow from the central primary chute appeared to dissipate very quickly leaving a velocity-deficit region along the y=0 plane. This is also quite evident from the profile plot. The fine-grid quadrant solution is found to provide much better qualitative predictions with the experimental data.

Total temperature contours inside the mixing duct are shown in figure 10 for the coarse- and fine-grid quadrant solutions. These contours share many of the same characteristics as the velocity contours of figure 7. Once again, the fine-grid solution indicates a stronger sidewall effect which causes the high-energy flow from the primary stream to separate from the core-flow region near the z=0 plane and move away from the xy-symmetry plane.

Figure 11 compares the total temperature contours at the duct exit plane with the experimental data. The coarse-grid quadrant solution shows two large hot-spots along the xy-symmetry plane and virtually no region of low total temperature near the sidewalls. The fine-mesh quadrant solution does not contain these errant hot-spots and seems to predict the size of the low total temperature region near the sidewall reasonably well. However, the magnitude of the total temperature predicted in this region is too low compared with the experimental data. As with the velocity contours, the fine-mesh half-chute calculation appears to be representative of the quadrant solution along the xz-symmetry plane.

The total temperature profiles at the duct exit plane along the z=0 and y=0 cut-lines are shown in figure 12. Once again, an extreme overprediction in total temperature is observed in the coarse-grid solution along the z=0 plane. In addition, the two hot-spots noted in the previous contour plot are also prevalent along this symmetry plane. The fine-grid quadrant solution provides good overall agreement with the experimental data, though the magnitude of the total temperature near the sidewalls is underpredicted.

Figure 13 displays the axial vorticity contours inside the mixing duct. As is shown, there is clearly strong vorticity along the trailing edge of the mixer lobes. However, even on finer scales, there is no evidence of vorticity from the secondary inlet influencing the flow within the mixing duct. It was originally thought that, as the freestream flow spilled over the external sidewall and into the secondary inlet, it rolled into a vortex. This vortex was then presumed to filter through the secondary chute nearest the sidewall and into the mixing duct, thus causing the formation of the velocity-deficit region.

With no evidence to support that theory, other sources were examined. Streamline traces indicate that the low energy flow in the velocity-deficit region originates from a wide range of points along the full-cold secondary chute. Figure 14 shows the static pressure contours along the sidewall of the mixing duct. Between x/L=0.25 and x/L=0.50, there is a mild pressure gradient from the top toward the center along the sidewall. It is believed that this gradient drives the low energy flow of the full-cold secondary chute toward the z=0 symmetry plane to form the velocity-deficit region.

Because of the good agreement of the fine-mesh quadrant solution with the experimental exit plane data, it is interesting to examine these results from a different perspective. Figure 15 once again compares the duct exit plane axial velocity and total temperature contours of the fine-mesh quadrant solution with the experimental data. However, this time the CFD solution has been mapped onto the experimental data locations using a nearest-point technique. This effectively coarsens the CFD to the same resolution of the experimental data.

Examining these contour plots, one immediately notes that the isolated circular regions of high-energy flow near z/H= $\pm$0.50 are no longer discernible, but have been replaced by broader contours which extend across a large portion of the duct width. This suggests that at this low resolution, the experimental data is likely missing many finer flow field details. Overall, the CFD appears capable of capturing the character of the flow, though slight differences in the magnitudes of the values prevent a more precise match of the contour shapes.

Table 2 compares the computed pumping and thrust with the experimental data. Values listed for the half-chute solutions were determined using only the half-chute domain on which the CFD was computed and do not include any corrections for the additional entrained mass flow near the sidewall. Therefore, one would expect the quadrant solutions to yield greater pumping than the corresponding half-chute solutions. This holds true for the fine-grid solutions, but not for the coarse-grid solutions — largely because in those solutions the mass conservation through the secondary inlet was poor. Comparison with the experimental data indicates that the fine-grid quadrant solution overpredicts the pumping by 2%. This may be due, at least in part, to the imposed freestream Mach number of 0.07 used in the CFD calculation. The gross thrust coefficient (C_{fg}) of the fine-grid quadrant solution compares very favorably with the experimental data.

Conclusions

In this study, CFD has been used to investigate the effect of the sidewall on flow within the mixing duct downstream of a lobed mixer-ejector nozzle. Solutions obtained from half-chute and full-quadrant simulations of the nozzle indicate that away from the sidewall the half-chute symmetry assumption appears to be valid. However, a full-quadrant simulation is needed to predict the formation of the low-energy region along the sidewall. Proper grid resolution was imperative to obtain accurate results. Predictions from the full-quadrant simulation with 65 points per mixer wavelength, an average y^+ of 1.5, and maximum grid stretching ratio of 1.3 within the mixing duct compared quite well with the available experimental data. Comparison of axial velocity and total temperature contours at the mixing duct exit plane exhibited good qualitative agreement, while profile comparisons of these same quantities demonstrated good quantitative agreement overall. However, the CFD solution was found to underpredict the total temperature near the duct sidewalls. No evidence was found to support the theory that the region of low-energy flow observed experimentally at the mixing duct exit plane was caused by a vortex feeding through one of the secondary chutes. However, the existence of a mild pressure gradient near the sidewall may cause flow from the slow moving secondary stream to pool near the xy-symmetry plane. These results indicate that CFD can be a valuable tool for analyzing the complicated flowfields of mixer-ejector nozzles.

References

1. Arney, L.D., Sandquist, D.L., Forsyth, D.W., and Lidstone, G.L., "Gen 2.0 Mixer/Ejector Nozzle Test at LSAF June 1995 - July 1996," NASA CR-2005-213334, February 2005.

2. Cooper, G.K., and Sirbaugh, J.R., "The PARC Distinction: A Practical Flow Simulator," AIAA Paper 90-2002, July 1990.

3. Chien, K.-Y., "Predictions of Channel and Boundary-Layer Flows with a Low-Reynolds-Number Turbulence Model," *AIAA Journal*, January 1982, Vol. 20, No. 1, pp. 33-38.

	Coarse Mesh		Fine Mesh	
	Half-Chute	Quadrant	Half-Chute	Quadrant
Primary Flow	20,160	196,224	38,658	359,346
Secondary Flow	57,195	555,345	78,324	804,690
Mixing Duct	28,548	237,900	178,266	1,734,042
External Flow	16,968	121,574	56,010	617,232
External Sidewall Flow	0	137,350	0	128,520
Plume	11,067	48,391	31,977	428,868
Total	133,938	1,296,784	383,235	4,072,698

Table 1: Distribution of Grid Points within Computational Domain.

	Coarse Mesh		Fine Mesh		Experiment
	Half-Chute	Quadrant	Half-Chute	Quadrant	
Pumping Ratio, ω	0.623	0.554	0.531	0.556	0.545
Thrust Coefficient, C_{fg}	1.076	1.102	0.990	0.981	0.980

Table 2: Performance Numbers.

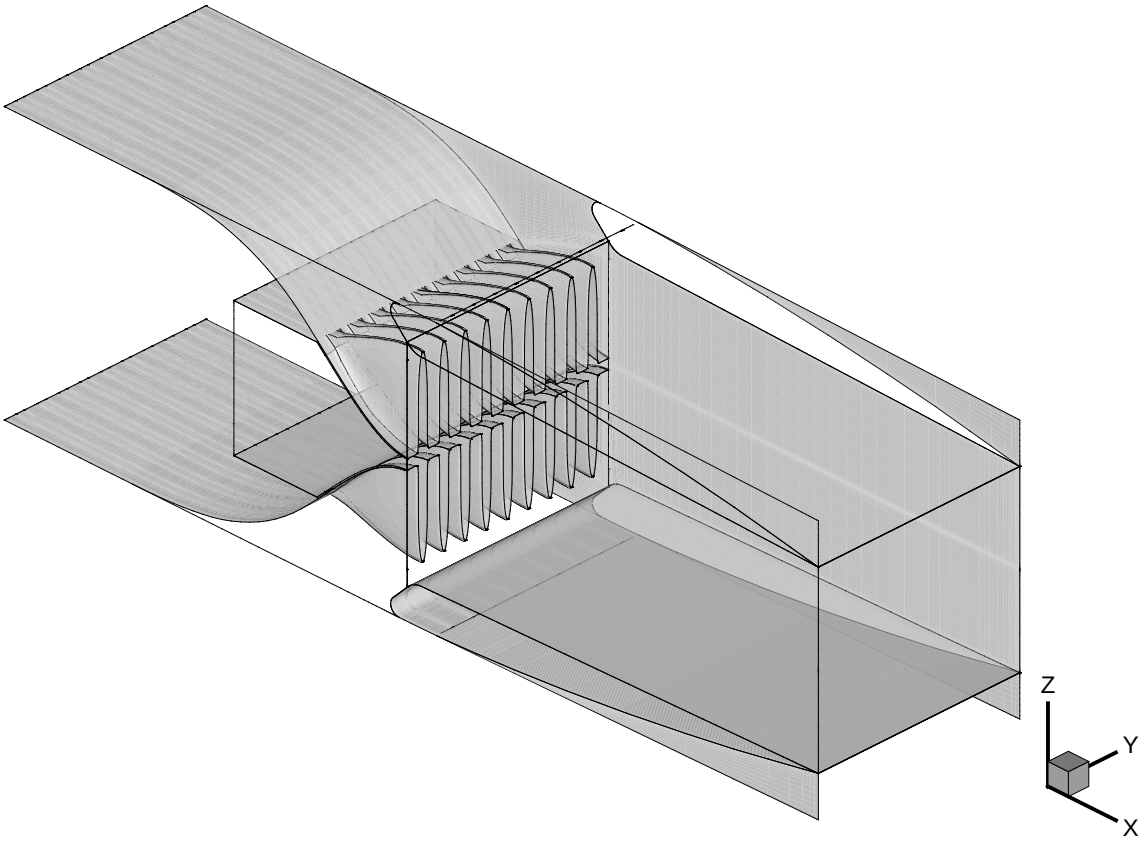

Figure 1: Schematic of Down Stream Mixer (DSM) Nozzle with Mixer #9 Installed.

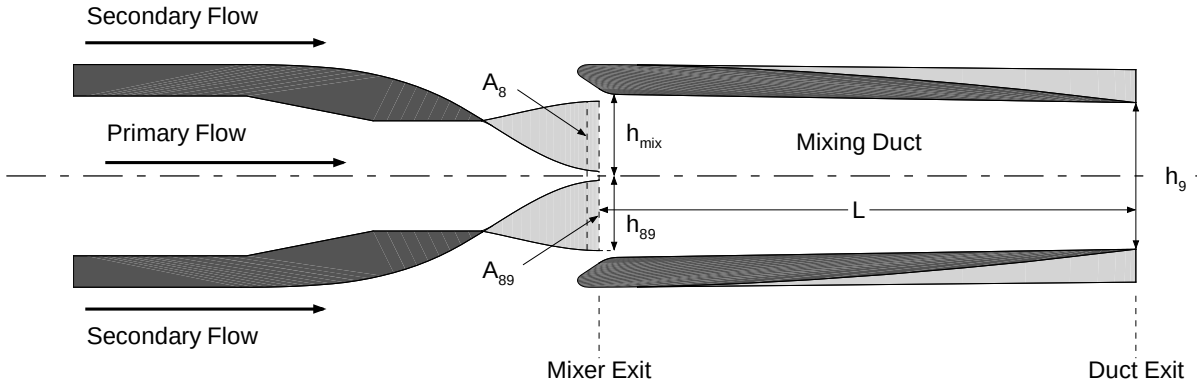

L	Length of Ejector Mixing Duct
W	Width of Ejector Mixing Duct
h_{89}	Height from Centerline to Peak of Primary Lobe at Mixer Exit
h_9	Overall Height at Mixing Duct Exit
h_{mix}	Half-Height of Ejector Mixing Duct at Flap Hinge Location

A_8	Primary Flow Mixer Throat Area
A_{89}	Primary Flow Mixer Exit Area
A_9	Overall Area at Mixing Duct Exit ($W*h_9$)
A_{mix}	Overall Area at Mixing Duct Entrance ($W*2h_{mix}$)
SAR	Suppressor Area Ratio (A_{mix}/A_8)
MAR	Mixing Duct Area Ratio (A_9/A_{mix})
CER	Chute Area Expansion Ratio (A_{89}/A_8)
PEN	Penetration (h_{89}/h_{mix})

Figure 2: Mixer-Ejector Nomenclature.

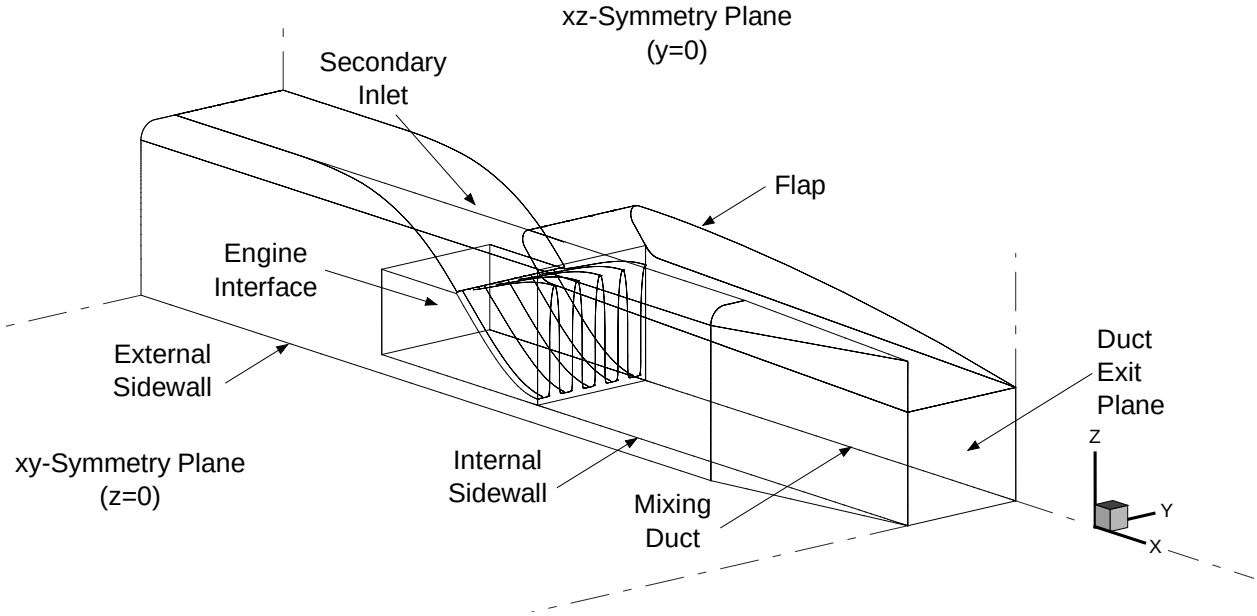

Figure 3: Schematic of Computational Domain for Quadrant Calculations.

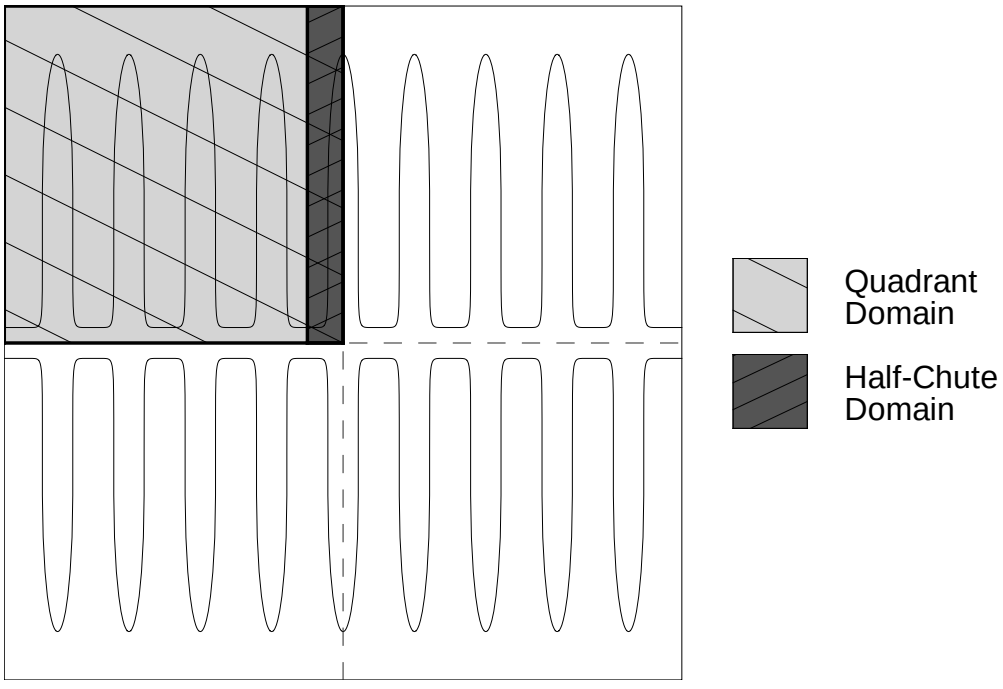

Figure 4: Comparison of Internal Flow Computational Domains for Quadrant and Half-Chute Calculations.

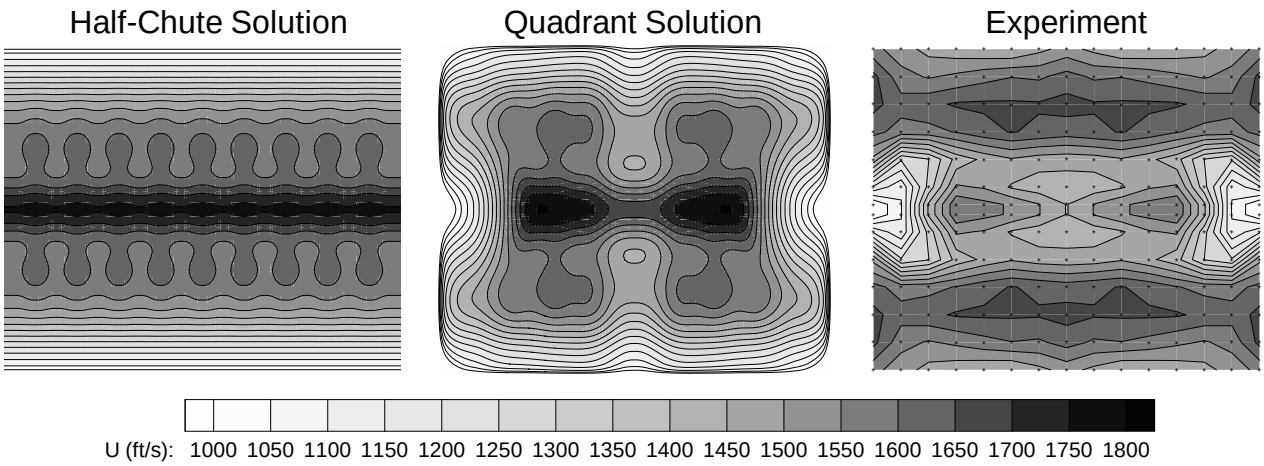

Figure 5: Coarse Mesh Predictions of Axial Velocity Contours at Duct Exit Plane.

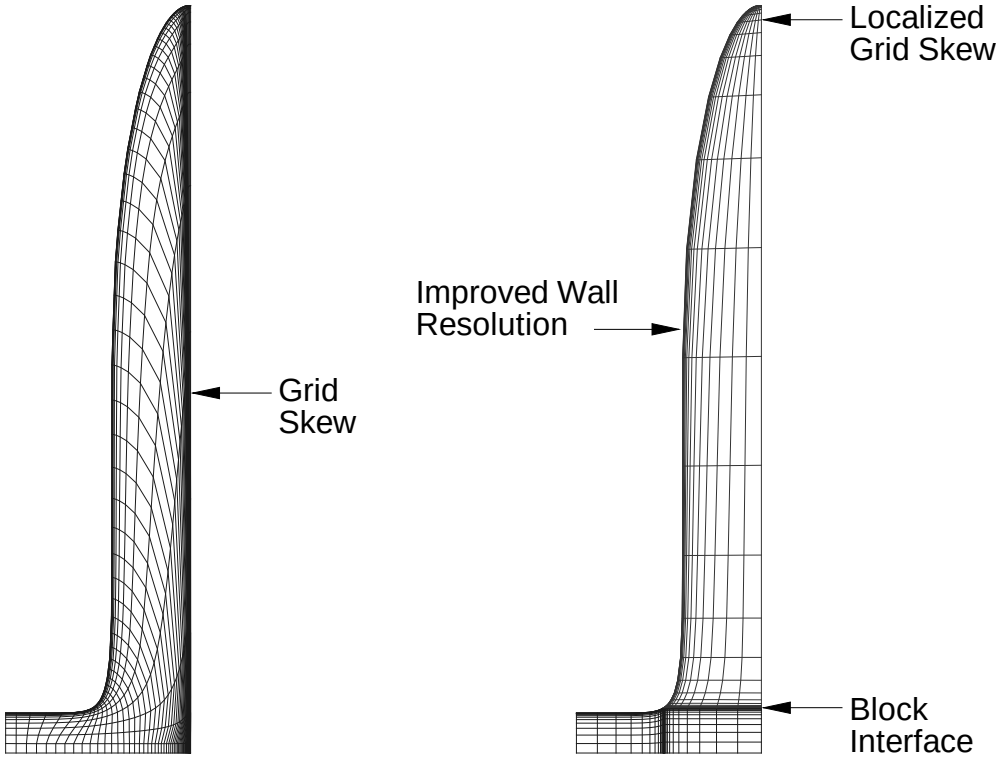

a) Single-Block Topology b) Multi-Block Topology

Figure 6: Schematic of Primary Chute Grid Topologies.
(Grids shown here have the same number of points.)

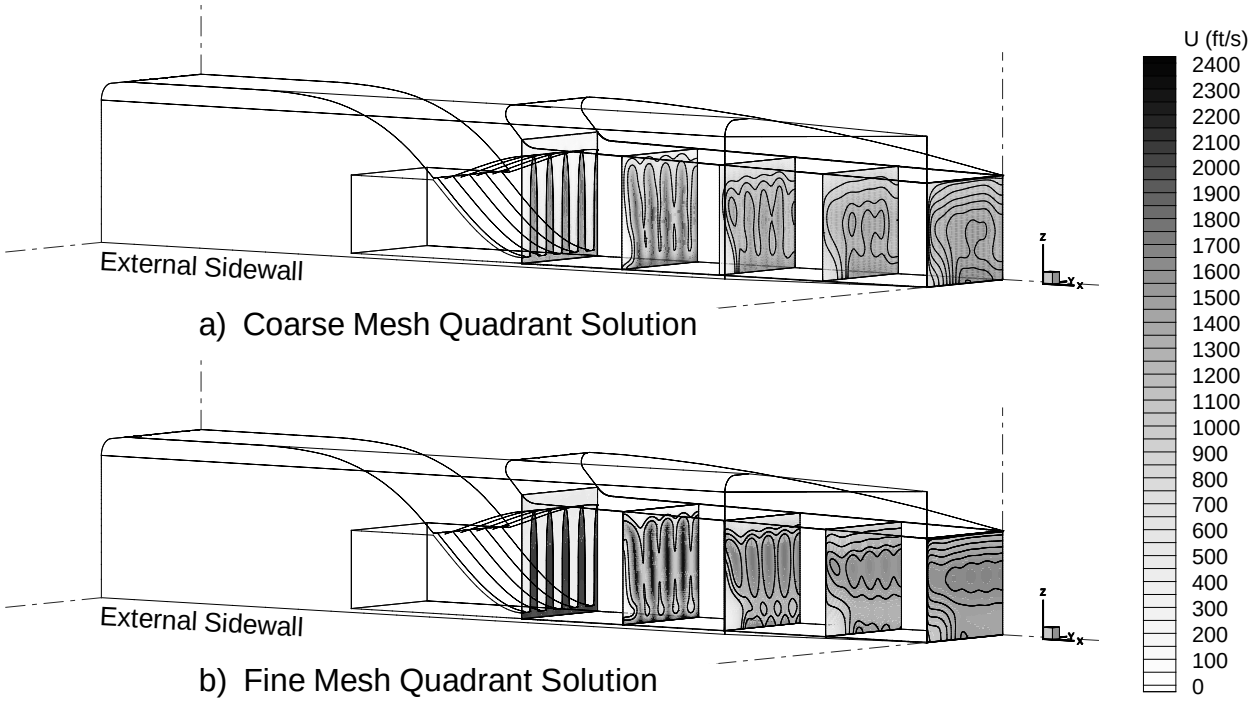

a) Coarse Mesh Quadrant Solution

b) Fine Mesh Quadrant Solution

Figure 7: Axial Velocity Contours Inside Mixing Duct for (a) Coarse and (b) Fine Mesh Quadrant Solutions.

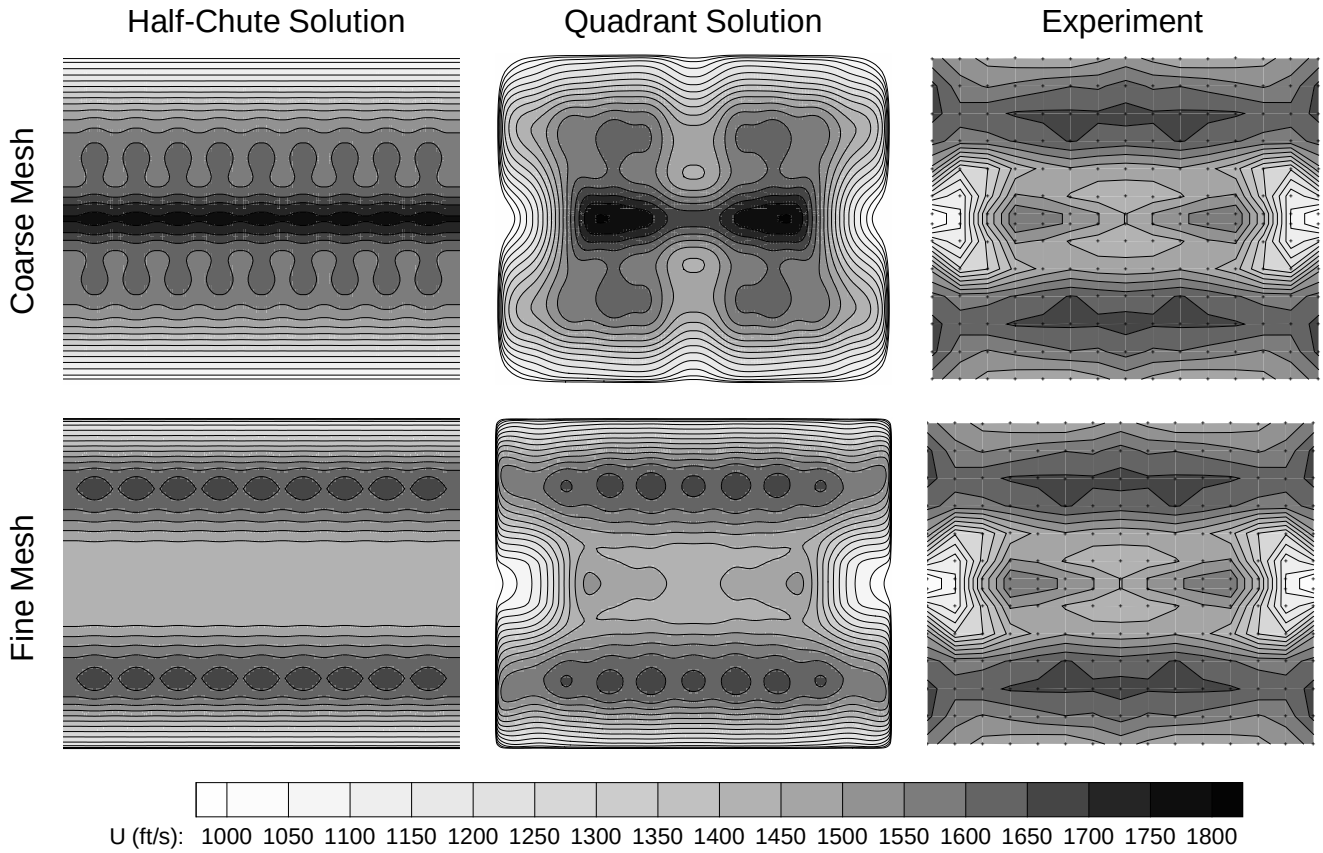

Figure 8: Axial Velocity Contours at Duct Exit Plane.

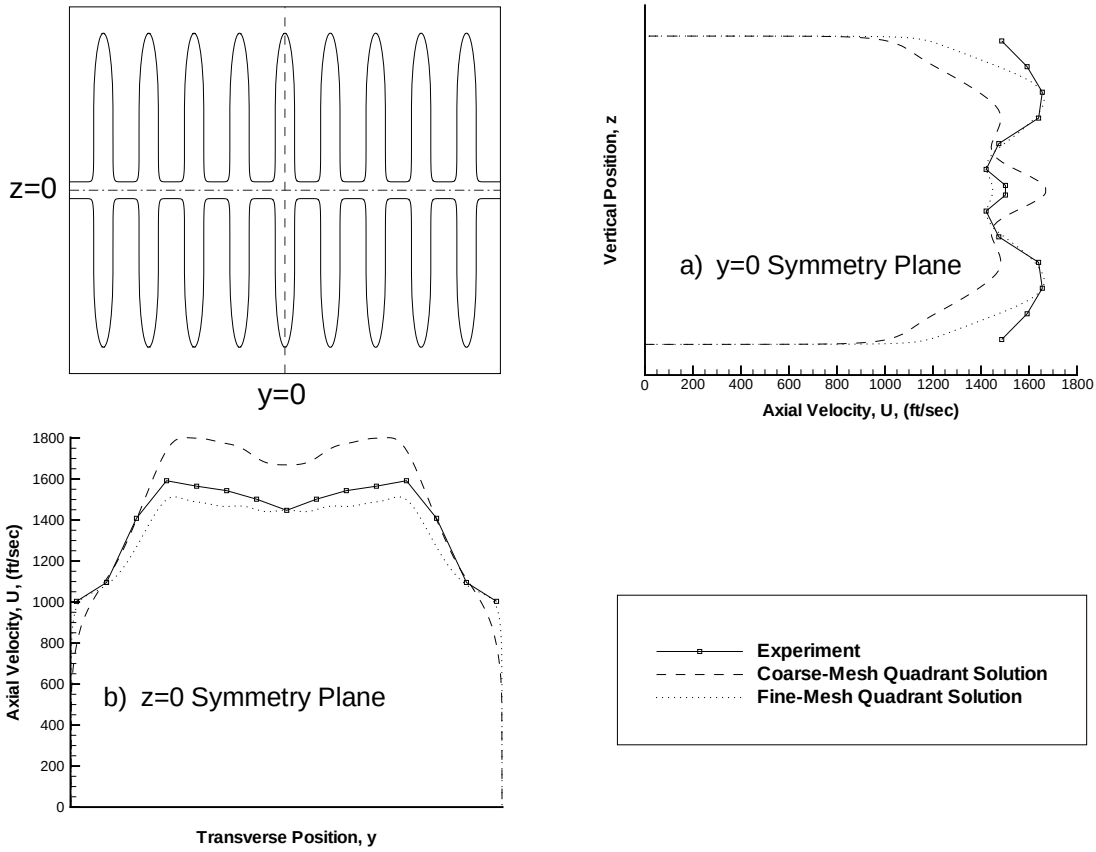

Figure 9: Comparison of Axial Velocity Profiles at Exit of Mixing Duct Along (a) y=0 and (b) z=0 Symmetry Planes.

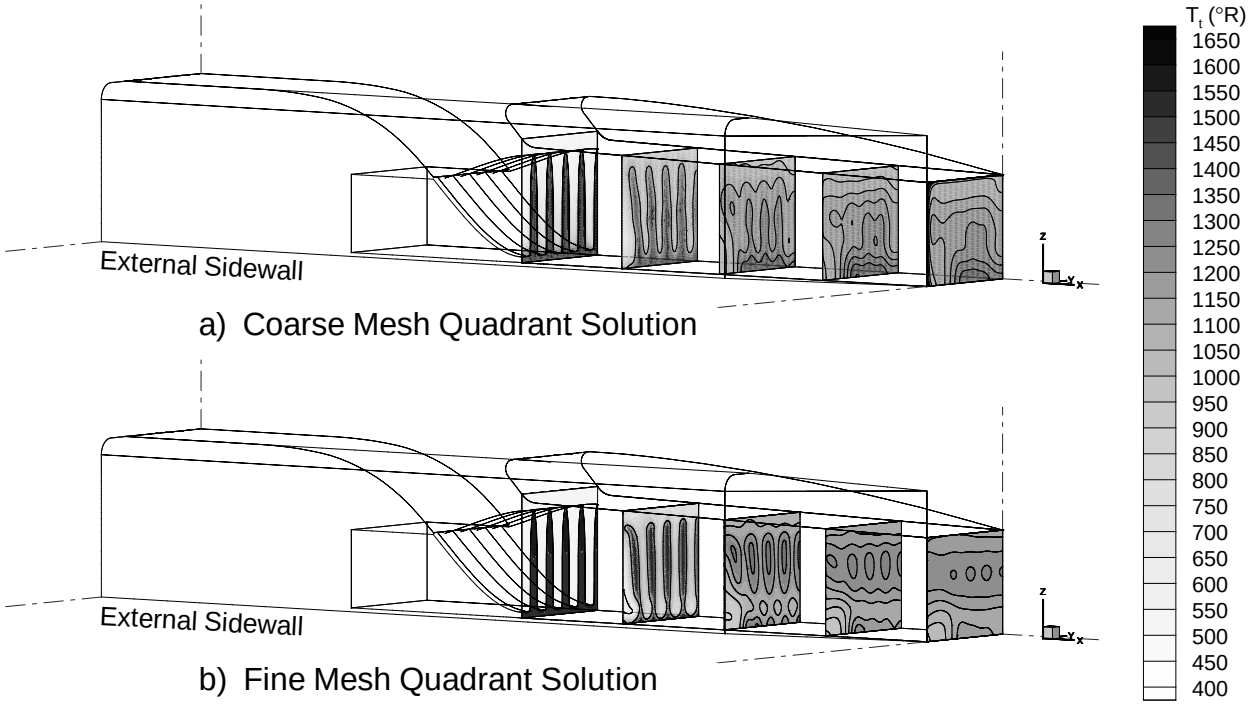

Figure 10: Total Temperature Contours Inside Mixing Duct for (a) Coarse and (b) Fine Mesh Quadrant Solutions.

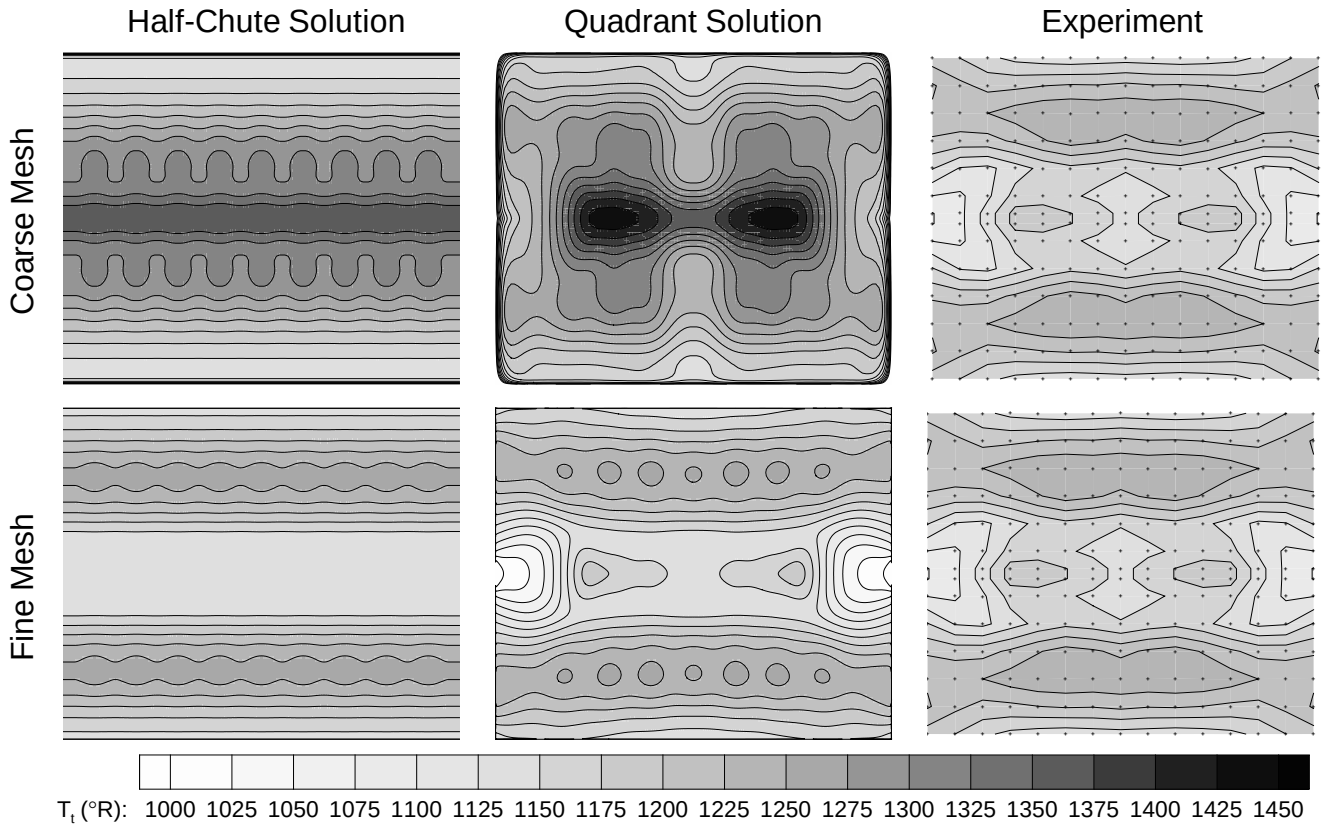

Figure 11: Total Temperature Contours at Duct Exit Plane.

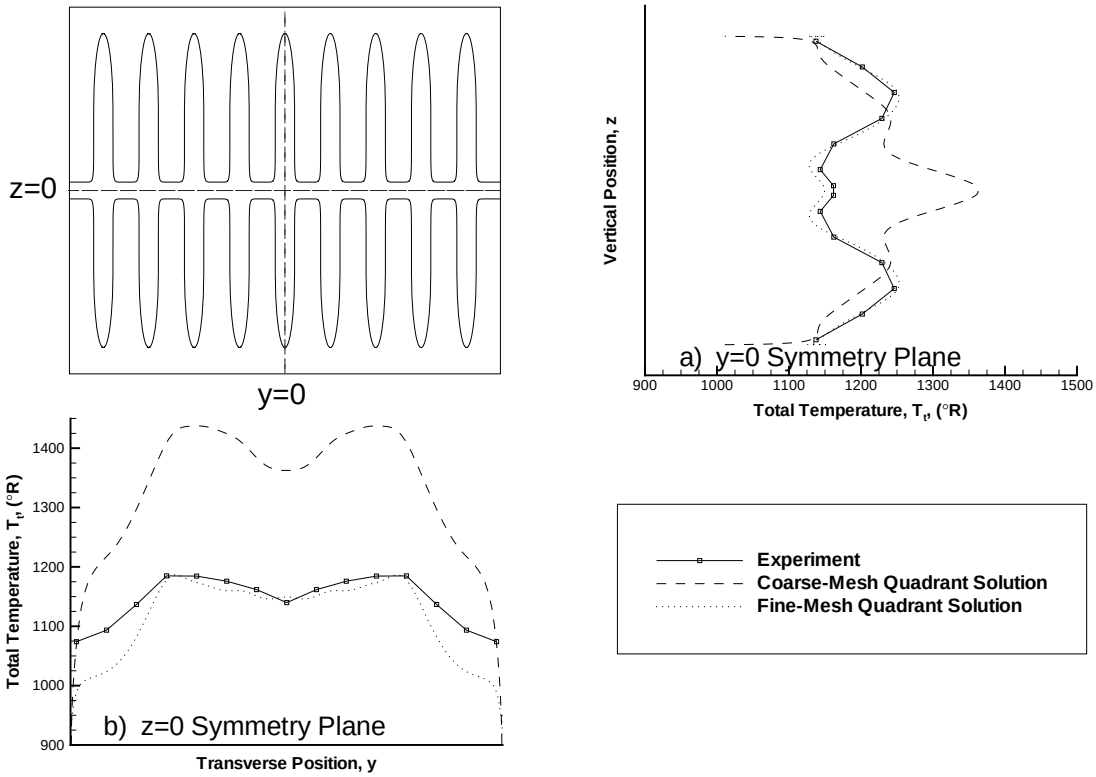

Figure 12: Comparison of Total Temperature Profiles at Exit of Mixing Duct Along (a) y=0 and (b) z=0 Symmetry Planes.

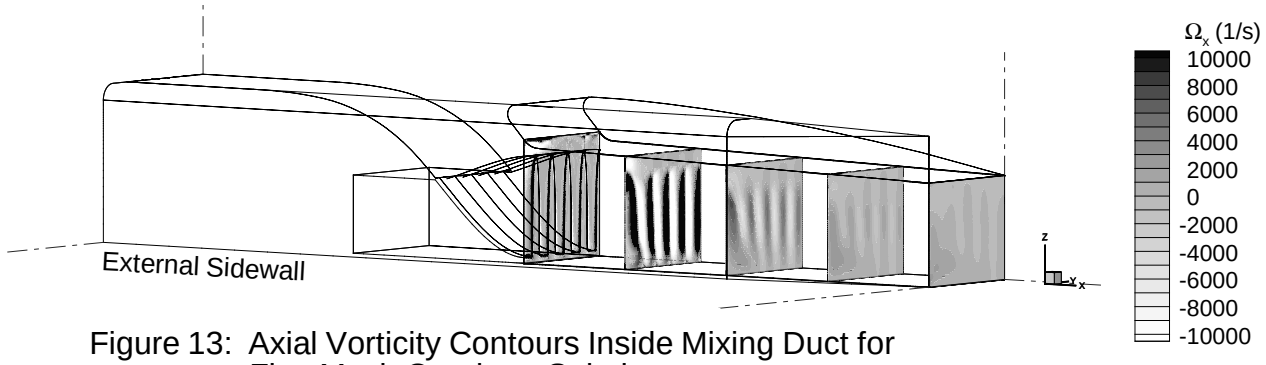

Figure 13: Axial Vorticity Contours Inside Mixing Duct for Fine Mesh Quadrant Solution.

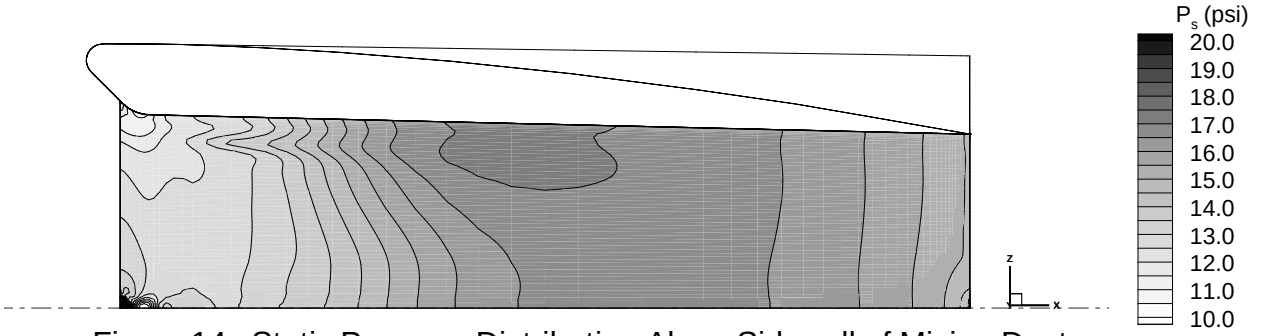

Figure 14: Static Pressure Distribution Along Sidewall of Mixing Duct.

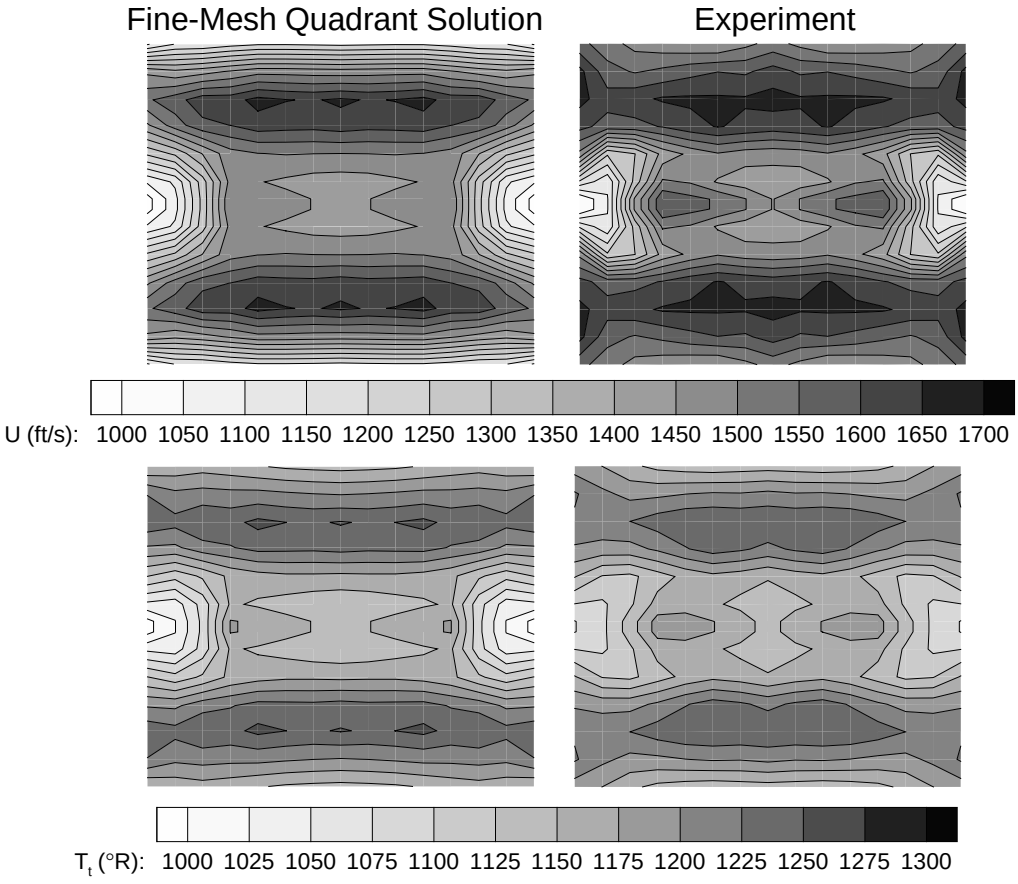

Figure 15: Comparison of Duct Exit Plane Contours with the Fine-Mesh Quadrant Solution Mapped onto Experimental Data Locations.

REPORT DOCUMENTATION PAGE

Form Approved
OMB No. 0704-0188

1. AGENCY USE ONLY (*Leave blank*)	2. REPORT DATE	3. REPORT TYPE AND DATES COVERED
	April 2005	Technical Memorandum

4. TITLE AND SUBTITLE

Quadrant CFD Analysis of a Mixer-Ejector Nozzle for HSCT Applications

5. FUNDING NUMBERS

WBS–22–714–09–47

6. AUTHOR(S)

Dennis A. Yoder, Nickolas J. Georgiadis, and John D. Wolter

7. PERFORMING ORGANIZATION NAME(S) AND ADDRESS(ES)

National Aeronautics and Space Administration
John H. Glenn Research Center at Lewis Field
Cleveland, Ohio 44135–3191

8. PERFORMING ORGANIZATION REPORT NUMBER

E–15069

9. SPONSORING/MONITORING AGENCY NAME(S) AND ADDRESS(ES)

National Aeronautics and Space Administration
Washington, DC 20546–0001

10. SPONSORING/MONITORING AGENCY REPORT NUMBER

NASA TM—2005-213602

11. SUPPLEMENTARY NOTES

This research was originally published internally as HSR071 in September 1999. Responsible person, Dennis A. Yoder, organization code RTN, 216–433–8716.

12a. DISTRIBUTION/AVAILABILITY STATEMENT

Unclassified - Unlimited
Subject Categories: 07, 34, and 05

Available electronically at http://gltrs.grc.nasa.gov

This publication is available from the NASA Center for AeroSpace Information, 301–621–0390.

12b. DISTRIBUTION CODE

13. ABSTRACT ***(Maximum 200 words)***

This study investigates the sidewall effect on flow within the mixing duct downstream of a lobed mixer-ejector nozzle. Simulations which model only one half-chute width of the ejector array are compared with those which model one complete quadrant of the nozzle geometry and with available experimental data. These solutions demonstrate the applicability of the half-chute technique to model the flowfleld far away from the sidewall and the necessity of a full-quadrant simulation to predict the formation of a low-energy flow region near the sidewall. The quadrant solutions are further examined to determine the cause of this low-energy region, which reduces the amount of mixing and lowers the thrust of the nozzle. Grid resolution and different grid topologies are also examined. Finally, an assessment of the half-chute and quadrant approaches is made to determine the ability of these simulations to provide qualitative and/or quantitative predictions for this type of complex flowfield.

14. SUBJECT TERMS

Exhaust nozzles; Ejectors; Jet mixing flow; Supersonic transports; Jet aircraft noise; Computational fluid dynamics

15. NUMBER OF PAGES

19

16. PRICE CODE

17. SECURITY CLASSIFICATION OF REPORT	18. SECURITY CLASSIFICATION OF THIS PAGE	19. SECURITY CLASSIFICATION OF ABSTRACT	20. LIMITATION OF ABSTRACT
Unclassified	Unclassified	Unclassified	